Epigallocatechin Gallate Affects the Structure of Chromatosomes, Nucleosomes and Their Complexes with PARP1

Tatiana V. Andreeva , Natalya V. Maluchenko , Anastasiya V. Efremenko , Alexander V. Lyubitelev , Ann N. Korovina , Dmitry A. Afonin , Mikhail P. Kirpichnikov , Vasily M. Studitsky * , Alexey V. Feofanov *

Posted Date: 29 August 2023

doi: 10.20944/preprints202308.1874.v1

Keywords: epigallocatechin gallate; nucleosome; chromatosome; poly(ADP-ribose) polymerase 1; spFRET microscopy

Article

Epigallocatechin Gallate Affects the Structure of Chromatosomes, Nucleosomes and Their Complexes with PARP1

Tatiana V. Andreeva [1], Natalya V. Maluchenko [1], Anastasiya V. Efremenko [2], Alexander V. Lyubitelev [1], Anna N. Korovina [1], Dmitry A. Afonin [1], Mikhail P. Kirpichnikov [1,2], Vasily M. Studitsky [1,3,*] and Alexey V. Feofanov [1,2,*]

[1] Faculty of Biology, Lomonosov Moscow State University, 119234, Moscow, Russia
[2] Shemyakin-Ovchinnikov Institute of Bioorganic Chemistry, Russian Academy of Sciences, 117997 Moscow, Russia
[3] Fox Chase Cancer Center, Philadelphia, PA 19111-2497 USA
* Correspondence: avfeofanov@yandex.ru to A.V.F.; vasily.studitsky@fccc.edu to V.M.S.

Abstract: The natural flavonoid epigallocatechin gallate (EGCG) has a wide range of biological activities including binding to nucleic acids; however, mechanisms of interaction of EGCG with DNA organized in chromatin have not been systematically studied. In this work, interaction of EGCG with chromatin in cells, and with nucleosomes and chromatosomes in vitro was studied using fluorescent microscopy and single particle Förster resonance energy transfer approaches, respectively. EGCG effectively penetrates into the nuclei of living cells and binds to DNA there. Interaction of EGCG with nucleosomes *in vitro* induces large-scale, reversible uncoiling of nucleosomal DNA that occurs without dissociation of DNA or core histones at sub- and low-micromolar concentrations of EGCG. EGCG does not reduce the catalytic activity of poly(ADP-ribose) polymerase 1 (PARP1), but causes modulation of the structure of the PARP1-nucleosome complex. EGCG significantly changes the structure of chromatosomes, but does not cause dissociation of the linker histone. Reorganization of nucleosomes and chromatosomes by EGCG might facilitate access of protein factors involved in DNA repair, replication and transcription to DNA and thus might contribute to the modulation of gene expression by EGCG that was reported earlier.

Keywords: epigallocatechin gallate; nucleosome; chromatosome; poly(ADP-ribose) polymerase 1; spFRET microscopy

1. Introduction

Epigallocatechin gallate (EGCG) is a natural flavonoid from the catechin group, which is found in abundance in green tea (Figure 1A). EGCG possesses a wide spectrum of biological activities including anti- and pro-oxidant, anti-inflammatory, anticancer and anti-infective (antiviral, antibacterial and antifungal) activities [1–4]. These activities of EGCG are observed at doses that are safe for humans [5–8] that stimulate numerous clinically oriented studies of EGCG.

Preprints (www.preprints.org) | NOT PEER-REVIEWED | Posted: 29 August 2023 doi:10.20944/preprints202308.1874.v1

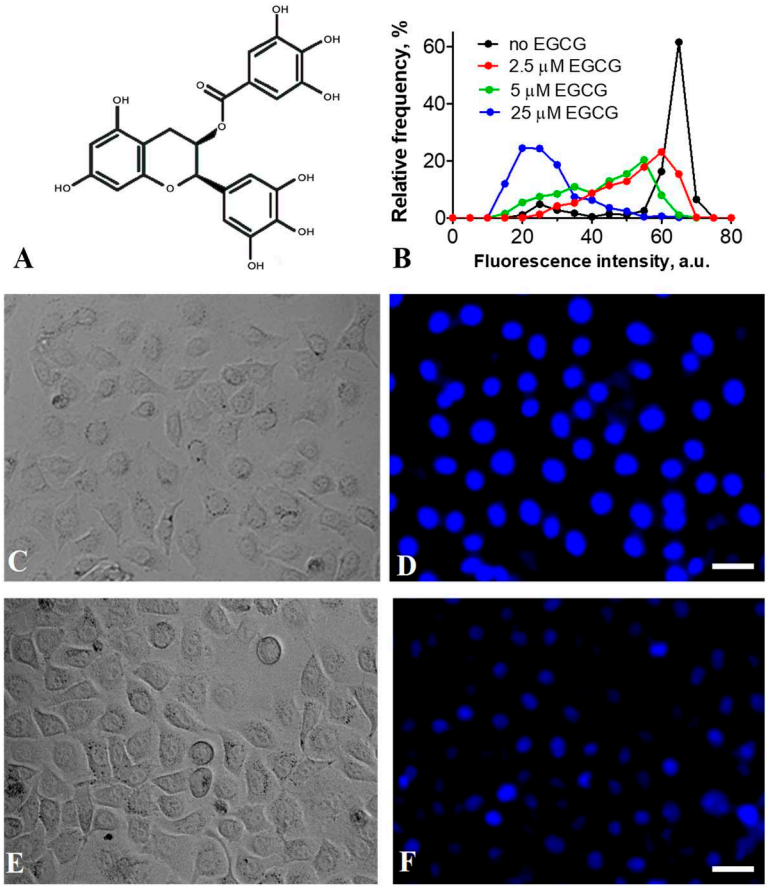

Figure 1. EGCG penetrates into nuclei of living cells and competes for the binding to DNA with Hoechst 33342. (A) Structure of EGCG. (B) Frequency distributions of cells by intensity of Hoechst 33342 fluorescence in the nuclei of HEK293 cells in the presence of different EGCG concentrations. Cells pre-incubated with 1 μM Hoechst 33342 for 3.5 h were incubated with indicated EGCG concentrations for 2.5 h in the complete medium. (C-F) Typical transmitted-light images of HEK293 cells (C, E) and fluorescent images of nuclei stained with Hoechst 33342 (D, F) in the absence (D) and presence (F) of 25 μM EGCG. Fluorescent images (D, F) were recorded under the same conditions; therefore, the signal intensities can be directly compared. Scale bar is 30 μm.

Mechanisms of EGCG action in mammalian cells include interactions with cell surface receptors, penetration into cytoplasm and interaction there with different signaling pathways, penetration into nucleus and modulation of gene expression [9]. Modulation of gene expression by EGCG is not accompanied by genotoxicity [10] and is assumed to be associated with inhibition of different transcription factors, DNA methyltransferase and class I histone deacetylases [9,11,12]. Nucleus-associated mechanisms of EGCG action include the poisoning of topoisomerases I and II and inhibition of poly(ADPribose)polymerase 1 (PARP1) [9,13–16]. PARP1 is a sensor of DNA damage, which recruits the DNA repair proteins to the DNA lesions [17]. It is considered as a target for the treatment of malignant neoplasms with homologous recombination deficiency [18]. PARP1 is involved in the regulation of gene expression, increasing the activity of transcription factors and acting on the proteins participating in methylation of DNA [19].

It was proposed that EGCG penetrates into the nucleus, and binds to DNA and RNA [20]. *In vitro* experiments confirmed that EGCG interacts with dsDNA, ssDNA and RNA [20]. The binding constant of the dsDNA-EGCG complex was measured to be $(2.3\pm0.8) \times 10^5$ M^{-1} [21]. According to molecular dynamics simulations, the EGCG interaction with dsDNA occurs by intercalation through the major groove and is characterized by a low DNA sequence specificity [22]. The intercalation of EGCG into dsDNA was confirmed experimentally [23,24]. At the same time, the binding of EGCG to

 doi:10.20944/preprints202308.1874.v1

nuclear DNA in living cells was not directly demonstrated, and the interaction of EGCG with chromatin was not systematically investigated.

To fill this gap, the present work focuses on the study of the chromatin-targeted activity of EGCG *in vitro*, namely, on the EGCG interaction with nucleosomes, chromatosomes and nucleosome complexes with PARP1. It was found that EGCG considerably reorganizes these structural units of chromatin and modulates the structure of PARP1-nucleosome complexes *in vitro*. Similar interactions could occur *in vivo*, since it was shown here that EGCG effectively penetrates into the nuclei of living cells and binds to DNA.

2. Results

2.1. Binding of EGCG to DNA in living cells

Earlier it was reported that Hoechst 33258, which binds to the minor groove of DNA, is displaced from the complexes with DNA in solution by different polyphenols, which are supposed to be either intercalators or minor groove-binding agents [25]. Hoechst 33342 is similar to Hoechst 33258 in the structure and in the mode of binding to DNA [26], but Hoechst 33342 penetrates easier in living cells, and its fluorescence is predominantly observed in the nuclei in the complexes with DNA (Figure 1C,D) [27]. Hoechst 33342 fluoresces in the blue region, while EGCG fluoresces in the UV range, and excitation of Hoechst 33342 fluorescence at the 405 nm wavelength does not result in the EGCG excitation. Taking into account these properties of Hoechst 33342 and EGCG, the fluorescence microscopy approach, which is based on the competition between Hoechst 33342 and EGCG for the binding to DNA in living cells, was applied to evaluate ability of EGCG to penetrate within the nuclei of cells and to interact with DNA there.

Our study shows that exposure of HEK293 cells, which were pre-incubated with Hoechst 33342, to EGCG leads to the concentration-dependent decrease in the fluorescence of DNA-Hoechst 33342 complexes (Figure 1B–F), suggesting that EGCG penetrates into the nuclei of living cells, interacts with DNA, and displaces Hoechst 33342.

The results of our study are consistent with previously published data on the intranuclear penetration of EGCG [28] and provide direct evidence of the interaction of EGCG with DNA in the living cells.

2.2. Experimental approaches for analysis of EGCG-nucleosome interaction

Since DNA in the nucleus is organized in nucleosomes, the question arises about the effect of EGCG interaction with DNA on the structure of nucleosomes and complexes of nucleosomes with nuclear proteins. To address this question, fluorescently labeled mononucleosomes were assembled and studied using electrophoretic mobility shift assay (EMSA) and Förster resonance energy transfer (FRET) fluorescent microscopy of single particles (spFRET microscopy).

Mononucleosomes were assembled using octamers of human histones and DNA containing 147-bp nucleosome positioning sequence 603 (NPS603), which was flanked with two 20- or 40-bp DNA linkers (see inserts in panels A, C, E of Figure 2). Three types of fluorescently labeled nucleosomes were prepared. Nucleosomes N(13,91) and N(35,112) with 20 bp-linkers had fluorescent labels (a donor-acceptor pair of labels, Cy3 and Cy5) within the nucleosome core at positions 13 and 91 bp (N(13,91)) or 35 and 112 bp (N(35,112)) from the beginning of NPS603. Cy3 and Cy5 labels are located close each other on the neighboring gyres of nucleosomal DNA and support efficient FRET [29]. Nucleosomes NL with two 40 bp-linkers had fluorescent labels in linkers at positions 10 bp before and 10 bp after NPS603. The different positions of the pair of labels enabled analysis of structural changes in the corresponding regions of a nucleosome with the FRET technique. Application of spFRET microscopy provided detection of structurally different subpopulations of nucleosome complexes with EGCG and PARP1. The technique is based on the measurement of FRET efficiency from single nucleosomes diffusing through the focus of laser beam in the highly diluted solution.

Preprints (www.preprints.org) | NOT PEER-REVIEWED | Posted: 29 August 2023 doi:10.20944/preprints202308.1874.v1

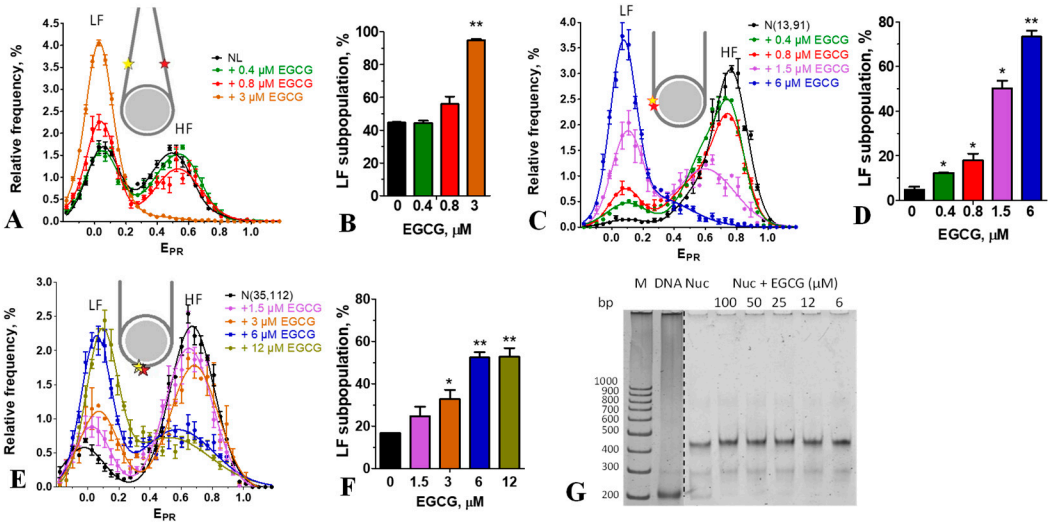

Figure 2. EGCG interaction with nucleosomes. (A, C, E) Frequency distributions of nucleosomes NL (A), N(13,91) (C) and N(35, 112) (E) by E_{PR} value in the absence and presence of different concentrations of EGCG (mean±SEM, n=3). Inserts – schematic structures of the studied nucleosomes with the positions of Cy3 and Cy5 labels marked with yellow and red asterisks, respectively. (B, D, F) Content of the low FRET (LF) subpopulation of nucleosomes NL (B), N(13,91) (D) and N(35, 112) (F) at different EGCG concentrations. The LF subpopulations were calculated on the basis of the corresponding E_{PR} –profiles. * - $p < 0.05$, ** - $p < 0.005$ as compared to nucleosomes without EGCG. (G) Analysis of the EGCG–nucleosome complexes by non-denaturing PAGE. M- marker, Nuc – nucleosomes. .

FRET is sensitive to structural changes, when the distance between the Cy3 and Cy5 labels varies from 4 to 9 nm. To further characterize large-scale structural changes in the nucleosomes and their complexes with EGCG and PARP1, EMSA was used.

2.3. Effect of EGCG on the structure of nucleosomes

NL nucleosomes were used to study the effect of EGCG on the conformation of nucleosomes within the linker DNA region. In agreement with the previously published data [30], spFRET microscopy revealed two subpopulations of NL, which differ in the conformation of linker DNA. These subpopulations of nucleosomes are recognized in the E_{PR}-profile (the graph showing the distribution of nucleosomes by the FRET efficiency) as low (LF) and high FRET (HF) peaks and are characterized by the different distance between DNA helices in the linker region, where the fluorescent labels are located. The binding of EGCG to NL noticeably affects the conformation of linker DNA at the EGCG concentration higher than 0.8 μM (Figure 2A) and leads to a decrease in the HF subpopulation of NL with a concomitant increase in the LF subpopulation (Figure 2A,B). Thus, the binding of EGCG to the nucleosome increases the distance between DNA helices in the linker region.

The study of N(13,91) and N(35, 112) nucleosomes shows that the effect of EGCG on the nucleosome structure is not limited to the linker region and extends to the core region (Figure 2C,E). For both N(13,91) and N(35, 112) nucleosomes, the E_{PR}-profiles are characterized by a dominant HF peak and a small LF peak in the absence of EGCG. The nucleosomes belonging to the HF peak have the intact structure with a close arrangement of DNA gyres on the histone octamer in the area of the fluorescent labels. LF subpopulations of N(13,91) and N(35, 112) nucleosomes may combine subnucleosomes, free nucleosomal DNA and nucleosomes with partially uncoiled nucleosomal DNA. "Breathing" or temporal spontaneous unwinding of 10-20 bp of nucleosomal DNA from the histone octamer near the nucleosome boundary [31] can also be detected in the case of N(13,91) with

Preprints (www.preprints.org) | NOT PEER-REVIEWED | Posted: 29 August 2023 doi:10.20944/preprints202308.1874.v1

the labels positioned close to the nucleosome boundary. Note that the proportion of the LF nucleosomes might vary from batch to batch of the assembled and purified nucleosomes.

Addition of EGCG to nucleosomes results in an increase in the LF subpopulation of N(13,91) and a decrease in their HF subpopulation that is accompanied by a shift of the HF peak maximum in the E_{PR}-profile (Figure 2C). The alterations of the E_{PR}-profile of N(13,91) appear at 0.4 μM and are more pronounced at higher EGCG concentrations (Figure 2C,D). The shift of the HF peak to lower E_{PR} values reflects a change in the conformation of nucleosomal DNA near the nucleosome boundary, which is accompanied by an increase in the distance between DNA gyres. This change is especially pronounced at ca. 1.5 μM EGCG (Figure 2C). An increase in the LF-subpopulation may correspond to either uncoiling of nucleosomal DNA from the histone octamer that involves at least 40-bp region at the beginning of NPS603 (as estimated previously [32]) and/or the disassembly (partial or total) of nucleosomes. An increase in EGCG concentration to 6 μM results in conversion of the majority of the N(13,91) nucleosomes into LF subpopulation (Figure 2C,D).

Similar structural changes were observed in the N(35, 112) nucleosomes interacting with EGCG (Figure 2E, F); however, they occurred at higher concentrations of EGCG as compared to the N(13,91) nucleosomes (Figure 2C,D), suggesting that a higher EGCG concentration is required to disturb the nucleosome structure in the region located 35 bp from the beginning of NPS603. An increase in EGCG concentration higher than 6 μM does not lead to additional changes in the structure of nucleosomes in the 35 and 112 bp regions (Figures 2E,F, and S1), indicating that saturation of EGCG binding to nucleosomes occurs at these concentrations. The data are in general agreement with the previously reported value of the dissociation constant of the EGCG-DNA complex (4.3 μM) [21].

According to spFRET data, ca. 52% of the nucleosomes had a disturbed conformation of nucleosomal DNA with an increased distance between DNA gyres in the region localized 35 bp from the beginning of NPS603 at the EGCG concentration higher 6 μM. In the remaining nucleosomes, a large-scale uncoiling of the nucleosomal DNA from the histone octamer occurred, involving at least 60 bp of NPS603 from either end of the nucleosome (as estimated previously [32]).

EMSA shows that incubation of nucleosomes with up to 100 μM of EGCG is not accompanied by dissociation of DNA from the histone octamer or by formation of subnucleosomes that have lost some histones (Figure 2G). This conclusion was confirmed by spFRET analysis, showing that after adding an excess of BSA, which binds EGCG [33], EGCG-nucleosome complexes dissociated, and the released nucleosomes restored the intact structure (Figure 3). BSA itself did not affect the nucleosome structure (Figure 3). Taken together, the data suggest that the structural changes induced by EGCG in nucleosomes occur without loss of histones and are reversible.

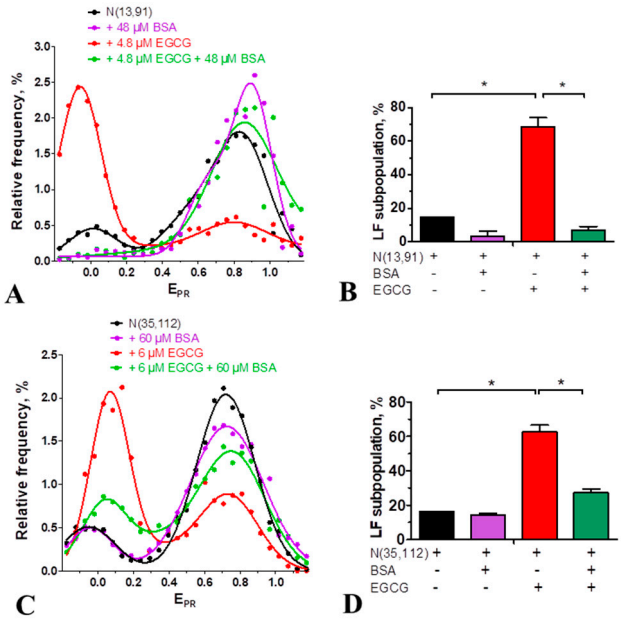

Preprints (www.preprints.org) | NOT PEER-REVIEWED | Posted: 29 August 2023 doi:10.20944/preprints202308.1874.v1

Figure 3. Reversibility of the EGCG-induced changes in a nucleosome structure. (A, C) Typical frequency distributions of nucleosomes N(13,91) (A) and N(35, 112) (C) by E_{PR} value in the absence and presence of EGCG (4.8 or 6 μM) and BSA (48 or 60 μM). (B, D) Content of the low FRET (LF) subpopulation of nucleosomes N(13,91) (B) and N(35, 112) (D) in the absence and presence of EGCG and BSA. The LF subpopulations were calculated from the corresponding E_{PR} –profiles. * - $p < 0.05$.

2.4. Efect of EGCG on the structure of chromatosomes

Linker histone H1 binds to nucleosomes and brings together the DNA linkers, forming chromatosomes [34]. In agreement with the data reported earlier [30], this structural transition is detected in the E_{PR}-profiles of chromatosomes formed by NL as an appearance of the single HF peak having a maximum at 0.55 or 0.59 depending on the type of the linker histone, H1.0 or H1.5, respectively, instead of two peaks (maxima at 0.07 and 0.45) characteristic for intact nucleosomes (Figure 4). Binding of EGCG to chromatosomes induces disturbance of the DNA conformation in the linker region observed as a shift of the peak in the E_{PR}-profile to the lower E_{PR} values (Figure 4). This shift is more pronounced at higher EGCG concentrations. Thus, at 6 μM EGCG (saturation of EGCG binding to nucleosomes), the peak maximum is localized at 0.17 or 0.11 for H1.0- or H1.5-containing chromatosomes, respectively (Figure 4). Since the maximum of the E_{PR}-profile of EGCG-NL complexes is at the lower E_{PR} value (0.07, Figure 4), and the differences in the positions of the peak maxima of EGCG-NL and EGCG-chromatosome complexes are significant ($p<0.05$), the disturbance of the chromatosome structure by EGCG, leading to an increase in the distance between the DNA helices in the linker region is unlikely to be accompanied by dissociation of the linker histones H1.0 and H1.5 even at the highest concentration of EGCG.

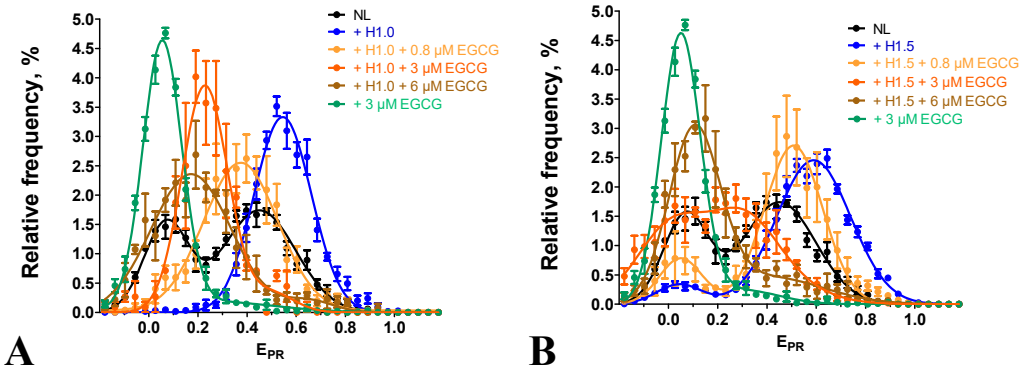

Figure 4. EGCG interaction with chromatosomes formed in the presence of linker histones H1.0 (A) and H1.5 (B). Frequency distributions by E_{PR} value (mean±SEM, n=3) are shown for nucleosomes NL and their complexes with EGCG (3 μM) as well as for chromatosomes and their complexes with EGCG (0.8, 3 and 6 μM).

2.5. Effect of EGCG on the PARP1-nucleosome complexes

Since EGCG is an inhibitor of PARP1 [16], we have studied the effect of EGCG on the interaction of PARP1 with nucleosomes.

In agreement with the published data [35], the PARP1 binding to nucleosomes results in the overall increase in the distance between DNA gyres on the histone octamer that is observed as a shift of the HF peak, a characteristic of the intact conformation of nucleosomal DNA, to the middle FRET region (MF, E_{PR}~0.45) in the E_{PR}-profile (Figure 5A). Binding to the nucleosome activates enzymatic activity of PARP1, and addition of the substrate, NAD^+, results in polyADPrybosylation (PARylation) of histones and PARP1 itself [35]. Eventually, PARylated PARP1 dissociates from the nucleosome because of the accumulation of the negative charge, and the released nucleosomes assume the native conformation of nucleosomal DNA, characterized by the reappearance of the characteristic HF peak in the E_{PR}-profile (Figure 5A) [35].

Preprints (www.preprints.org) | NOT PEER-REVIEWED | Posted: 29 August 2023 doi:10.20944/preprints202308.1874.v1

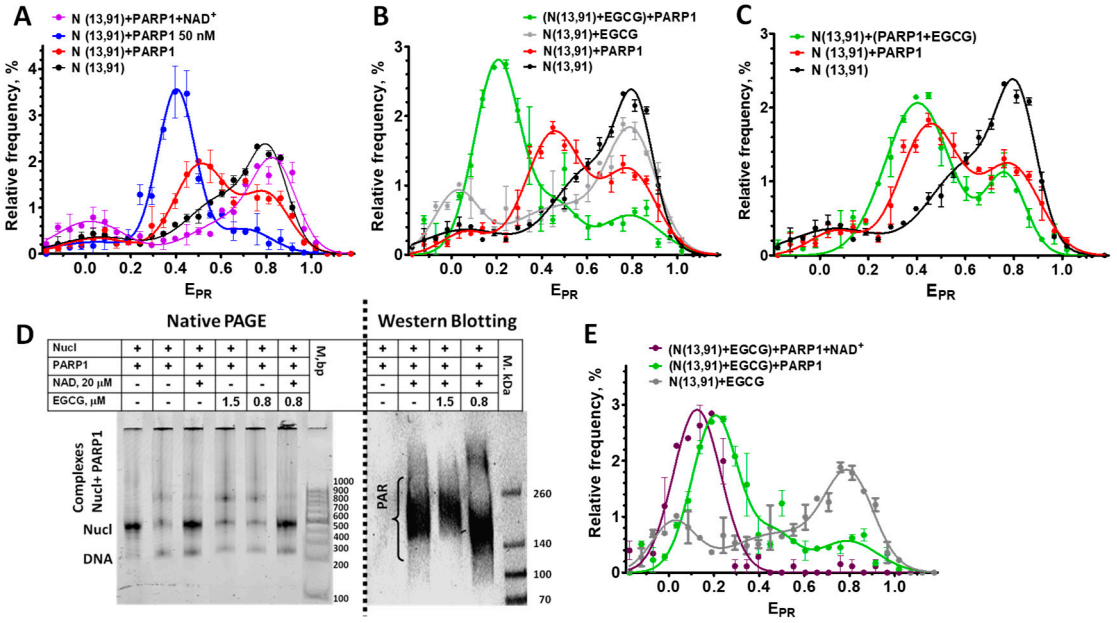

Figure 5. Effect of EGCG on the interactions of nucleosomes with PARP1. (A) E_{PR}-profiles of nucleosomes N(13,91) and their complexes with PARP1 (20 or 50 nM) or with PARP1 (20 nM) after addition of NAD^+ (20 μM). (B, C) E_{PR}-profiles of nucleosomes N(13,91) and their complexes either with EGCG (0.8 μM) or with PARP1 (20 nM), or with PARP1 (20 nM) in the presence of EGCG (0.8 μM). PARP1 was added to nucleosomes pre-incubated (15 min) with EGCG (B) or simultaneously with EGCG (C). (D) Analysis of the complexes of nucleosomes with PARP1, EGCG and NAD^+ by non-denaturing PAGE or by Western blotting with the use of antibodies to PAR. (E) E_{PR}-profiles of the complexes of nucleosomes N(13,91) with either EGCG (0.8 μM) or with EGCG (0.8 μM) and PARP1 (20 nM) or with PARP1 and EGCG after addition of NAD^+ (20 μM). (A-C, E) Data are mean±SEM (n=3).

To study the effect of EGCG on the PARP1-nucleosome interaction, including changes in the PARP1 affinity for the nucleosome, the concentration of PARP1 (20 nM) was selected at which ca. 65% of nucleosomes were recruited in the complex (Figure 5A–C). Concentration of EGCG (0.8 μM) was selected, which was eightfold less than the concentration of the saturated binding (ca. 6 μM) but still induced the noticeable changes in the E_{PR}-profile of N(13,91) nucleosomes (Figure 5B). Addition of PARP1 (20 nM) to the preformed EGCG-nucleosome complexes results in the appearance of the new peak (E_{PR}=0.2) in the E_{PR}-profile that is positioned between the LF peak of EGCG-nucleosomes complexes and the MF-peak of PARP1-nucleosome complexes (Figure 4B). This peak of the EGCG-nucleosome-PARP1 complexes comprises ca. 67% of the detected particles indicating that the fraction of nucleosomes that form the complexes with PARP1 was not changed in the presence of EGCG. Thus, EGCG does not disturb the binding of nucleosomes to PARP1, but strongly affects the structure of the complexes, further increasing the distance between DNA gyres on the histone octamer as compared to the PARP1-nucleosome complex. An increase in the EGCG concentration up to 10 μM also does not reduce the binding of PARP1 to nucleosomes (see Figures 5D and S2).

When PARP1 (20 nM) was preincubated with EGCG (0.8 μM) and added to nucleosomes, the effect of EGCG on the structure of the complexes was less pronounced, with a smaller increase in the distance between DNA gyres as compared to the preformed EGCG-nucleosome complexes interacting with PARP1 (compare Figure parts 4B and C). The data suggest that PARP 1 binds to nucleosomes faster than EGCG, and, being bound to nucleosomes, interferes with the binding of EGCG to nucleosomal DNA.

Addition of NAD^+ to the EGCG-nucleosome-PARP1 complexes resulted in dissociation of PARP1 from nucleosomes (see native PAGE in Figure 5D). This dissociation was induced by autoPARylation of PARP1 that occurred efficiently at sub- and low- micromolar concentrations of

 doi:10.20944/preprints202308.1874.v1

EGCG (see WB in Figure 5D). An increase in the EGCG concentration to 10 μM did not interfere with NAD^+-induced dissociation of PARP1 from nucleosomes, indirectly indicating preservation of the autoPARylation activity of PARP1 even at the saturating concentration of EGCG (Figure S2). Therefore, the EGCG interaction with nucleosomes does not prevent the PARP1 binding to nucleosomal DNA, which is required for the enzyme activation, and EGCG does not inhibit the catalytic activity of PARP1.

Dissociation of PARylated PARP1 from nucleosomes in the presence of EGCG did not restore the E_{PR}-profile that was observed before the PARP1 binding to EGCG-nucleosome complexes (Figure 5E). Instead, the single peak was observed with the maximum shifted to the E_{PR} value of 0.13, indicating that all the nucleosomes adopted a similar conformation with increased distance between DNA gyres. It can be supposed that the association of EGCG with additional binding sites that become available in nucleosomes reorganized by PARP1 enhances the effect of EGCG on the structure of the released nucleosomes.

3. Discussion

Limited bioavailability and reduced absorption rate of EGCG result in the limited (micromolar) concentration of EGCG in the plasma and tissues [36]. Therefore, achievable concentrations of EGCG in cells can determine the spectrum of biological effects of EGCG and their effectiveness.

Our experiments show that EGCG penetrates into the nuclei of cells and bind there with DNA (Figure 1). Nuclear concentration of EGCG is unknown, but can be roughly estimated from our experiments. Intranuclear concentration of EGCG is high enough to compete with Hoechst 33342 for the binding to DNA even at the low-micromolar extracellular concentrations of EGCG (Figure 1B). Bright fluorescent signal of Hoechst 33342 in cells indicates that the concentration of the dye bound to DNA is higher than 0.1 μM. The binding constants of DNA to dyes of the Hoechst family and EGCG are ca. 2×10^8 M^{-1} [37] and 2.3×10^5 M^{-1} [21]. Therefore, to displace Hoechst 33342 from the complexes with DNA, the intranuclear concentration of EGCG should be thousand times higher than that of Hoechst 33342 and achieve ca. 100 μM. This high intranuclear accumulation of EGCG explains the previous observation that "nucleic acids extracted from EGCG treated human cancer cells were catechin colored" [20]. Very high distribution coefficient (the ratio of intracellular to extracellular concentration) of EGCG is probably a reason why consumption of green tea is useful in the case of various human diseases [38–40] in spite of the limited bioavailability of EGCG. EGCG effectively interacts with nucleosomal DNA at sub- and low-micromolar concentrations (Figures 2 and 4), while inhibition of DNA methyltransferase occurs at sub-micromolar concentrations of EGCG [9], and class I histone deacetylases are inactivated by EGCG at 50-200 μM [12]. Poisoning of topoisomerases I and II requires interaction of EGCG with DNA and is realized at micromolar concentrations of EGCG [9,13–15]. Intercalation in DNA creates an increased local concentration of EGCG, which may contribute to the enhancement of inhibition of enzymes interacting with chromatin. Our experiments with BSA (Figure 3) show that EGCG intercalated into DNA can easily migrate from DNA to EGCG-binding proteins.

Our results show that EGCG can affect the activity and interaction of certain enzymes, for example, PARP1 to nucleosomes in a complex way. Thus, although affinity of PARP1 to nucleosomes is not reduced in the presence of EGCG, the catechin causes modulation of the structure of the PARP1-nucleosome complex (Figure 5) that in turn could affect the assembly of the DNA repair complex, the process triggered by the PARP1-mediated synthesis of PAR polymers. The effect of EGCG on the catalytic activity of PARP1 is intricate. PARP1 activity was not changed at sub- and low-micromolar concentrations of EGCG as probed by WB and EMSA, which mainly addressed the autoPARylation activity of PARP1 (Figure 5). Previously, inhibition of PARP1 by EGCG was observed *in vitro* using the assay based on the analysis of the PARylation of immobilized histones, i.e. trans-PARylation activity of PARP1 [16]. Probably, this discrepancy occurs because EGCG differentially affect trans- and auto- PARylation activities of PARP1, similar to some other factors reported earlier [41].

Nucleosomes and chromatosomes are basic structural units of chromatin, and our data show that EGCG reorganizes them *in vitro* at sub- and low-micromolar concentrations (Figures 2 and 4).

 doi:10.20944/preprints202308.1874.v1

EGCG-induced conformational changes occur in both linker and nucleosomal DNA and lead to a large-scale uncoiling of nucleosomal DNA from the histone octamer which, depending on the EGCG concentration, involves up to 60 bp from each of the two nucleosome boundaries. This reorganization of nucleosomes is not accompanied by dissociation of either DNA or core histones and is completely reversible after EGCG dissociation from the nucleosome (Figures 2G and 3). This suggests a low probability of irreversible structural changes caused by EGCG in chromatin and, at least in part, might explain the lack of genotoxicity of EGCG [10]. The reorganization of chromatosomes by EGCG, which very likely occurs without dissociation of the linker histone (Figure 4), suggests that the tight packing of heterochromatin may be also disrupted by EGCG in the cells.

Since not more than one EGCG molecule binds per 3-6 base pairs of DNA [20], the maximum number of EGCG molecules bound to a nucleosome assembled on DNA of 227 bp length is 38-75, and it is achieved at the saturation of the binding at 6 μM EGCG. Assuming a linear relationship between the concentration and the number of bound EGCG molecules, the noticeable disturbance of the nucleosome and chromatosome structure, which is observed at ca. 1 μM EGCG (Figures 2 and 4), occurs at the number of bound EGCG molecules of 6-12 per nucleosome (1 EGCG molecule per 18-36 bp). Can the number of DNA-bound EGCG molecules be high enough to destabilize the structure of chromatin in cells? Average intranuclear concentration of DNA is ca. 10 mg/ml or 15 mM (in base pairs) assuming that all DNA is double stranded [42]. On the basis of the binding constant of the dsDNA-EGCG complex, one can calculate that the equilibrium is totally shifted to the DNA bound state even at nanomolar intranuclear concentrations of EGCG and even if not more than 0.1% of nuclear DNA is accessible for the interaction with the catechin. Therefore, destabilization of the chromatin structure will occur at the nuclear concentration of EGCG of 400-800 μM or 4-8 μM, depending on 100 or 1% of DNA in the chromatin is accessible for interaction, respectively. Since nuclear concentration of EGCG can be as high as 100 μM (see above), EGCG-induced destabilization of chromatin structure is a very likely mechanism of EGCG action. The EGCG-induced reorganization of nucleosomes and chromatosomes could facilitate access of protein factors involved in DNA repair, replication and transcription to nucleosomal DNA and thus contribute to the observed modulation of gene expression [9].

4. Materials and Methods

4.1. Cellular experiments

HEK293 cells (the Russian collection of cell cultures, the Institute of Cytology RAS, Saint Petersburg, Russia) were grown in Dulbecco's modified Eagle's medium DMEM/F12 (Paneco, Russia) supplemented with 10 % fetal bovine serum (HyClone, Utah, USA) and 2 mM L-glutamine (complete medium) and transplanted two times a week. A day before the experiments, cells were transferred in 96-well plates ((2.0±0.4)×10^4 cells per well) and grown in the complete medium (37 °C, 5% CO_2). Cells were incubated with 1 μM Hoechst 33342 for 3.5 h and further incubated with EGCG (2.5-25 μM) for 2.5 h in the complete medium. Control cells were incubated with 1 μM Hoechst 33342 for 6 h in the complete medium. Cells were imaged with ZOE Fluorescent Cell Imager (Bio-Rad, Singapore). Fluorescence was excited and recorded in the 335-375 and 415-451 nm spectral ranges, respectively. Fluorescent images of cells were analyzed with Image J software (National Institute of Health, Bethesda, Maryland, USA) using the "Analyze particles" plugin. Sampling size varied from 400 to 600 cells. Experiments were repeated in triplicate.

4.2. DNA

The DNA templates were obtained by polymerase chain reaction (PCR) using a plasmid containing the 603–42A nucleosome positioning sequence [43] and fluorescently labeled primers. The DNA templates of 187-bp length were obtained using primers published previously [44].

The 227-bp DNA template was obtained in two-step PCR as described earlier [30] using the forward 5′-CACCGGCACGAGGGCCCGGTTC-3′ primer and the reverse 5′ -

Preprints (www.preprints.org) | NOT PEER-REVIEWED | Posted: 29 August 2023 doi:10.20944/preprints202308.1874.v1

ACTTTCTGGCAAGAAAATGAGCT-3′ primer in the first step and the following fluorescently labeled primers in the second step:

forward- 5′-ACACGGCGCACTGCCAACCCAAACGACACCT[Cy3-dT]GCACGAG-3′;

reverse- 5′-TAAGGCGAATTCACAACTTTTTGGCAAGAAT[Cy5-dT]ATGAGCT-3′.

Purification and extraction of the PCR products from 2% agarose gel was performed using QIAquick Gel Extraction Kit (Qiagen, Venlo, The Netherlands).

4.3. Proteins

Recombinant human histones were obtained in a bacterial expression system. The canonical genes of human histones H2A, H2B, H3 and H4 were cloned into a pET-3-based vector and expressed in *E. coli* cells at 37 °C. Expression of histone H4 was carried out in strain Rosetta 2(DE3). Histones H2A, H2B and H3 were expressed in strain BL21(DE3). An overnight culture was inoculated into Luria broth (LB) medium with 100 μg/ml ampicillin (and 24 μg/ml chloramphenicol for Rosetta 2(DE3)). Isopropyl-beta-D-thiogalactopyranoside (IPTG, 0.4 mM) was added to cells, when their optical density reached 0.6 optical units/cm at 600 nm. In 2 h after induction, the cells were harvested by centrifugation (3200 ×*g*, 30 min), washed with water, and frozen. Purification of individual histones was performed using the procedure described earlier [45] with the option of sequential stacking of HiTrap Q FF (5 ml) and HiTrap SP HP (5 ml) columns.

Expression vector based on pET3 plasmid containing gene of human linker histone H1.5 was kindly provided by S. Dimitrov. Rosetta2(DE3) *E. coli* cells were transformed with this vector by electroporation. An overnight culture of transformed cells was inoculated into liquid LB medium containing 100 μg/ml ampicillin. Cells were grown at 37 °C until optical density of 0.6 optical units/cm at 600 nm. Protein expression was induced by adding IPTG (0.5 mM), and after 4 h incubation, cells were harvested by centrifugation (3900 ×*g* for 20 min at 4 °C), washed with PBS buffer, and shock-frozen with liquid nitrogen. Purification of H1.5 was performed using the procedure described earlier [45] using sequentially stacked HiTrap Q FF (5 ml) and HiTrap SP FF (5 ml) ion exchange columns. Protein-containing fractions were collected, concentrated and dialyzed against SAU-1000 buffer (400 mM NaOAc, 10 mM EDTA, 100 mM lysine-HCl, 1 M NaCl, 6 M urea, 5 mM β-mercaptoethanol (β-ME)). Protein solution was applied onto a Hi-Prep Sephacryl 16/60 S200 HR gel filtration column equilibrated with SAU-1000 buffer. Protein elution was performed with the same buffer. Protein-containing fractions were collected, dialyzed against 20 mM Tris-HCl pH 8.0 at 4 °C for 24 h and concentrated.

Recombinant linker histone H1.0 from *Xenopus laevis* was expressed in *E. coli* as described earlier [46].

Expression plasmid pET-28-PARP1 bearing gene of human PARP1 fused with hexahistidine tag at the N-terminus was kindly provided by J.M. Pascal. The plasmid was transformed into *E. coli* cells (strain Rosetta2 (DE3) pLysS). Cells were grown on LB agar plates containing 50 μg/ml kanamycin and 35 μg/ml chloramphenicol overnight at 37 °C. Then, a single colony was inoculated into LB media supplemented with the same antibiotics, grown overnight at 37 °C and transferred into the large volume of LB medium (1-4.5 L) at hundredfold dilution. Cells were cultivated at 37 °C in the presence of kanamycin (50 μg/ml), chloramphenicol (35 μg/ml) and benzamide (10 mM) until the optical density of 0.8-1.0 optical units/cm at 600 nm. After chilling cells on ice, PARP1 synthesis was induced with 0.2 mM IPTG in the presence of 0.1 mM $ZnCl_2$. Cells were incubated at 16 °C for 16 h, centrifuged at 3900 ×*g* for 30 min, resuspended in a storage buffer (25 mM HEPES pH 8.0, 500 mM NaCl, 0.5 mM tris(2-carboxyethyl)phosphine (TCEP), 10 mM benzamide) and frozen at -80 °C or used for protein purification.

All the further purification steps were accomplished at 4 °C on ice. Cells were lysed using an ultrasonic disintegrator with the preliminary addition of 0.1% NP-40 and protease inhibitors (1 mM PMSF, 0.5 μg/ml leupeptin, 0.7 μg/ml pepstatin A, 0.5 μg/ml antipain, protease inhibitor cocktail P2714 (Sigma-Aldrich, Merck, Germany) and 1 mM benzamidine). The lysate was centrifuged at 18000 ×*g* for 1.5 h, filtered (0.22 μm), and applied to the HiTrap Chelating column (Cytiva, USA) for affinity chromatography. All the chromatography steps were performed with AKTA Purifier

 doi:10.20944/preprints202308.1874.v1

chromatography system (Cytiva, USA). Next, the column was washed sequentially with three buffers (25 mM HEPES pH 8.0, 0.5 mM TCEP, 20 mM imidazole, protease inhibitors) containing 500, 1000 and again 500 mM NaCl. PARP1 was eluted with a buffer containing 25 mM HEPES pH 8.0, 500 mM NaCl, 0.5 mM TCEP, 250 mM imidazole. The eluate was diluted with a salt-free buffer (50 mM Tris-HCl pH 7.0, 1 mM EDTA, 0.1 mM TCEP) by 2.5 times and filtered. Then, the sample was applied to the HiTrap heparin column (Cytiva, USA) and washed with buffer A (50 mM Tris-HCl pH 7.0, 200 mM NaCl, 1 mM EDTA, 0.1 mM TCEP) and increasing gradient (from 0 to 100%) of buffer B (50 mM Tris-HCl pH 7.0, 1 M NaCl, 1 mM EDTA, 0.1 mM TCEP). Fractions containing PARP1 (analyzed by SDS-PAGE) were pooled, concentrated with Amicon Ultra 4 unit, and centrifuged to get rid of insoluble components. Finally, protein was applied to a HiPrep 16/60 Sephacryl S-200 HR gel filtration column and eluted with a gel filtration buffer (25 mM HEPES pH 8.0, 150 mM NaCl, 1 mM EDTA, 0.1 mM TCEP). Purity and homogeneity of the obtained fractions were analyzed by SDS-PAGE. PARP1-containing fractions were concentrated, flash-frozen and stored at -80 °C.

4.4. Nucleosomes

The assembly of histone octamers was performed according to the protocol of denaturation-refolding followed by gel filtration on Superdex 200 [47]. Purity of histone octamer was analyzed by sodium dodecyl sulfate–polyacrylamide gel electrophoresis. Concentration of histone octamer was measured with UV spectrophotometry.

Histone octamers and DNA templates were used to assembly nucleosomes in the course of dialysis against decreasing concentration of NaCl as described earlier [48]. Assembled nucleosomes were analyzed by the electrophoresis in non-denaturing 4.5% polyacrylamide gel (acrylamide:bisacrylamide 39:1; 0.5× TBE buffer, pH 8.0).

For experiments with PARP1, nucleosomes were isolated from the gel by extraction in a buffer containing 10 mM HEPES-NaOH (pH 8.0), 0.2 mM EDTA, 0.2 mg/ml bovine serum albumin (BSA) and stored at 4°C.

4.5. Preparation of complexes for spFRET analysis

EGCG (Sigma-Aldrich, Merck, Germany) was dissolved in 100% DMSO at the concentration of 5 mM and stored at -20 °C. EGCG (0.4-50 μM) was mixed with nucleosomes (1 nM) in a buffer (150 mM KCl, 5 mM $MgCl_2$, 1 mM β-ME, 20 mM Tris-HCl, pH=7.5) and incubated for 20 min at room temperature (RT). In experiment with BSA, BSA (48 or 60 μM) was added to the preformed EGCG-nucleosome complexes and the mixture was incubated for 20 min at RT. In the experiments with linker histones, nucleosomes were incubated with H1.0 (15 nM) or H1.5 (7.4 nM) for 15 min in low-adhesion tubes; a half of the solution was mixed with EGCG (0.8-6 μM) and was further incubated for 20-30 min at RT. The DMSO concentration in samples with nucleosomes was less than 1% and did not affect the structure of nucleosomes as verified with the spFRET microscopy (Figure S3).

In experiments with PARP1, EGCG (0.8 μM) was mixed with nucleosomes (1 nM) in the TB150 buffer (20 mM Tris-HCl (pH 7.9), 5 mM $MgCl_2$, 150 mM KCl, 1 mM β-ME) and incubated for 15 min at RT; PARP1 (20 or 50 nM) was added to this mixture or to nucleosomes (1 nM), and the samples were incubated for 30 min at RT. Preincubated samples containing PARP1 were mixed with NAD+ (20 μM) and incubated for 45 min at RT. Alternatively, PARP1 (20 nM) was mixed with EGCG (0.8 μM), incubated for 15 min at RT and then incubated with nucleosomes (1 nM) for 30 min at RT.

4.6. spFRET microscopy

spFRET measurements were carried out using the LSM 710-Confocor3 system (Carl Zeiss, Aalen, Germany) with the C-Apochromat water-immersion lens (40×, NA1.2). Samples were placed into the 12-well silicon chamber (ibidi Gmbh, Martinsried, Germany) attached to a cover glass. Details of measurements were described earlier [48]. [12]. Fluorescence of single nucleosomes and their complexes diffusing through the laser focus was excited at the 514.5 nm wavelength (0.2 μW) and recorded in the 530–635 (Cy3) and 635–800 nm (Cy5) ranges during 10 min at the 3 ms integration

 doi:10.20944/preprints202308.1874.v1

time. The confocal diaphragm was set to 1 Airy disk. The proximity ratio (E_{PR}) was calculated for each detected particle as described earlier [48]. Data samples were presented as frequency distributions of nucleosomes by the E_{PR} value (E_{PR}-profiles) and averaged (mean±SEM, n=3, 3000-16000 particles) over three independent experiments.

E_{PR}-profiles were fitted as a superposition of one, two or three Gaussian peaks. Selection of the number of Gaussian peaks was made after the comparison of the alternative variants by the root-mean-square deviation. The content of specific subpopulations of nucleosomes was calculated as the ratio of the areas under specific Gaussian peaks to the total area under the E_{PR}-profile (as a percentage). Results of the analysis were averaged. To determine the significance of the differences, an unpaired two-tailed t-test was used.

4.7. Electrophoresis

For the electrophoresis aimed to study integrity of EGCG-nucleosome complexes, EGCG (6-100 μM) was added to nucleosomes (60 nM) in 0.01 M buffer for dialysis (10 mM NaCl, 10 mM Tris-HCl (pH 7.9), 0,1% NP40, 0,2 mM EDTA, 5 mM β-ME), incubated for 20 min, mixed with sucrose (final concentration 10%) and loaded into the 4% polyacrylamide gel. Electrophoresis was performed in the HE buffer (10 mM HEPES-NaOH pH 8.0, 0,2 mM EDTA) at +4˚C at 80 V.

In the PARP1-related studies, nucleosomes (2-3 nM) were preincubated with EGCG (0.8- 10 μM, 15 min, 25°C) and further incubated with PARP1 (20 or 50 nM) or with PARP1 and NAD+ (20 μM) in the TB150 buffer (45 min, 25°C). The probes were subjected to electrophoresis in 4% polyacrylamide gel (acrylamide: bisacrylamide 59:1; 0.2×TBE buffer) at 120 V for 90 min. Ladder GeneRuler 100 bp (Thermo Fisher Scientific, Waltham, MA, USA) was used as a marker.

Fluorescent imaging of the gels was performed using the Amersham Typhoon RGB imager (GE Healthcare Bio Sciences AB, Uppsala, Sweden).

4.8. Western blotting

Probes (20 μl) for WB were prepared as for electrophoresis (see above), mixed with 5 μl of the 5× loading buffer (312 mM Tris-HCl pH 6.8, 10% SDS, 25 % β-ME, 0.05% bromophenol blue) and then heated to 95°C for 5-10 min. After that the probes were subjected to electrophoresis in the 4-12% bis-Tris gradient gel in the Tris-glycine/SDS running buffer (25 mM Tris-HCl, 192 mM glycine and 0.1% SDS, pH 8.6.) at 130 V for 1 h at RT. The protein transfer on the supported nitrocellulose membrane (Bio-Rad) was performed in the transfer buffer (50 mM MOPS, 50 mM Tris-HCl, 1 mM EDTA, 3.5 mM SDS) with 20% ethanol at 4°C (350 mA, 2 h). The membrane was incubated for 60 min in the PBS-T solution (2.7 mM KCl, 8 mM Na_2HPO_4, 2 mM KH_2PO_4, 37 mM NaCl, 0.5% Tween 20) supplemented with the 5% skimmed milk (prepared from dry powder) and washed twice with the 1×PBS-T solution for 5 min. Then the membrane was incubated with mouse monoclonal antibodies against PAR (catalog number ab14459, Abcam, USA) for 1 h in PBS-T/5% milk, washed, incubated with the secondary anti-mouse antibodies conjugated with horseradish peroxidase (Bio-Rad, Hercules, CA, USA) for 1 h in the PBS-T/5% milk solution and washed again. Immunodetection was performed using the Chemidoc reader (Bio-Rad) and the Super Signal West Pico chemiluminescent substrate (Thermo Fisher Scientific, Waltham, MA, USA) for 3 min.

Supplementary Materials: The following supporting information can be downloaded at the website of this paper posted on Preprints.org. Figure S1: Frequency distributions of nucleosomes N(35, 112) by E_{PR} value in the absence and presence of 12 and 50 μM EGCG (mean±SEM, n=3); Figure S2: Analysis of the complexes of nucleosomes with PARP1, EGCG and NAD+ by non-denaturing PAGE; Figure S3: Frequency distributions of nucleosomes by E_{PR} value in the absence and presence of 2% DMSO (mean±SEM, n=3).

Author Contributions: conceptualization, N.V.M., V.M.S. and A.V.F.; data curation, T.V.A., N.V.M., A.V.E., A.V.L. and A.V.F.; formal analysis, N.V.M., A.V.E., M.P.K. and A.V.F; funding acquisition, T.V.A., N.V.M., A.N.K., V.M.S., A.V.E., A.V.F.; investigation, T.V.A., N.V.M., A.V.E., A.V.L., A.N.K., and D.A.A.; methodology, N.V.M., A.V.E., A.N.K., D.A.A. and A.V.F.; project administration, N.V.M., V.M.S. and A.V.F.; resources, N.V.M., M.P.K., V.M.S. and A.V.F.; supervision, N.V.M., M.P.K., V.M.S. and A.V.F.; writing—original draft,

T.V.A., N.V.M., A.V.E., A.N.K., D.A.A., M.P.K., V.M.S. and A.V.F.; writing—review and editing, N.V.M., M.P.K., V.M.S. and A.V.F. All authors have read and agreed to the published version of the manuscript.

Funding: This work was funded by the Russian Science Foundation (project no. 21-74-20018). Cellular experiments were funded by the Ministry of Science and High Education of Russian Federation (project no. 0101-2019-0015).

Institutional Review Board Statement: not applicable.

Informed Consent Statement: not applicable.

Data Availability Statement: The data presented in this study are available on request from the corresponding authors. The data are not publicly available due to local regulations.

Conflicts of Interest: The authors declare no conflict of interest.

References

1. Tang, G.; Xu, Y.; Zhang, C.; Wang, N.; Li, H.; Feng, Y. Green Tea and Epigallocatechin Gallate (EGCG) for the Management of Nonalcoholic Fatty Liver Diseases (NAFLD): Insights into the Role of Oxidative Stress and Antioxidant Mechanism. *Antioxidants (Basel)* **2021**, *10*, doi:10.3390/ANTIOX10071076.
2. Payne, A.; Nahashon, S.; Taka, E.; Adinew, G.M.; Soliman, K.F.A. Epigallocatechin-3-Gallate (EGCG): New Therapeutic Perspectives for Neuroprotection, Aging, and Neuroinflammation for the Modern Age. *Biomolecules* **2022**, *12*, doi:10.3390/BIOM12030371.
3. Steinmann, J.; Buer, J.; Pietschmann, T.; Steinmann, E. Anti-Infective Properties of Epigallocatechin-3-Gallate (EGCG), a Component of Green Tea. *Br J Pharmacol* **2013**, *168*, 1059–1073, doi:10.1111/BPH.12009.
4. Gan, R.Y.; Li, H. Bin; Sui, Z.Q.; Corke, H. Absorption, Metabolism, Anti-Cancer Effect and Molecular Targets of Epigallocatechin Gallate (EGCG): An Updated Review. *Crit Rev Food Sci Nutr* **2018**, *58*, 924–941, doi:10.1080/10408398.2016.1231168.
5. Isbrucker, R.A.; Edwards, J.A.; Wolz, E.; Davidovich, A.; Bausch, J. Safety Studies on Epigallocatechin Gallate (EGCG) Preparations. Part 2: Dermal, Acute and Short-Term Toxicity Studies. *Food and Chemical Toxicology* **2006**, *44*, 636–650, doi:10.1016/J.FCT.2005.11.003.
6. Hu, J.; Webster, D.; Cao, J.; Shao, A. The Safety of Green Tea and Green Tea Extract Consumption in Adults – Results of a Systematic Review. *Regulatory Toxicology and Pharmacology* **2018**, *95*, 412–433, doi:10.1016/J.YRTPH.2018.03.019.
7. Isbrucker, R.A.; Edwards, J.A.; Wolz, E.; Davidovich, A.; Bausch, J. Safety Studies on Epigallocatechin Gallate (EGCG) Preparations. Part 3: Teratogenicity and Reproductive Toxicity Studies in Rats. *Food and Chemical Toxicology* **2006**, *44*, 651–661, doi:10.1016/J.FCT.2005.11.002.
8. Mah, E.; Chen, O.; Liska, D.J.; Blumberg, J.B. Dietary Supplements for Weight Management: A Narrative Review of Safety and Metabolic Health Benefits. *Nutrients 2022, Vol. 14, Page 1787* **2022**, *14*, 1787, doi:10.3390/NU14091787.
9. Kim, H.S.; Quon, M.J.; Kim, J. a. New Insights into the Mechanisms of Polyphenols beyond Antioxidant Properties; Lessons from the Green Tea Polyphenol, Epigallocatechin 3-Gallate. *Redox Biol* **2014**, *2*, 187–195, doi:10.1016/J.REDOX.2013.12.022.
10. Isbrucker, R.A.; Bausch, J.; Edwards, J.A.; Wolz, E. Safety Studies on Epigallocatechin Gallate (EGCG) Preparations. Part 1: Genotoxicity. *Food and Chemical Toxicology* **2006**, *44*, 626–635, doi:10.1016/J.FCT.2005.07.005.
11. Ciesielski, O.; Biesiekierska, M.; Balcerczyk, A. Epigallocatechin-3-Gallate (EGCG) Alters Histone Acetylation and Methylation and Impacts Chromatin Architecture Profile in Human Endothelial Cells. *Molecules* **2020**, *25*, doi:10.3390/MOLECULES25102326.
12. Thakur, V.S.; Gupta, K.; Gupta, S. Green Tea Polyphenols Causes Cell Cycle Arrest and Apoptosis in Prostate Cancer Cells by Suppressing Class I Histone Deacetylases. *Carcinogenesis* **2012**, *33*, 377–384, doi:10.1093/CARCIN/BGR277.
13. López-Lázaro, M.; Calderón-Montaño, J.M.; Burgos-Morón, E.; Austin, C.A. Green Tea Constituents (-)-Epigallocatechin-3-Gallate (EGCG) and Gallic Acid Induce Topoisomerase I- and Topoisomerase II-DNA Complexes in Cells Mediated by Pyrogallol-Induced Hydrogen Peroxide. *Mutagenesis* **2011**, *26*, 489–498, doi:10.1093/MUTAGE/GER006.
14. Suzuki, K.; Yahara, S.; Hashimoto, F.; Uyeda, M. Inhibitory Activities of (-)-Epigallocatechin-3-O-Gallate against Topoisomerases I and II. *Biol Pharm Bull* **2001**, *24*, 1088–1090, doi:10.1248/BPB.24.1088.
15. Bandele, O.J.; Clawson, S.J.; Osheroff, N. Dietary Polyphenols as Topoisomerase II Poisons: B Ring and C Ring Substituents Determine the Mechanism of Enzyme-Mediated DNA Cleavage Enhancement. *Chem Res Toxicol* **2008**, *21*, 1253–1260, doi:10.1021/TX8000785.

16. Alqahtani, S.; Welton, K.; Gius, J.P.; Elmegerhi, S.; Kato, T.A. The Effect of Green and Black Tea Polyphenols on BRCA2 Deficient Chinese Hamster Cells by Synthetic Lethality through PARP Inhibition. *Int J Mol Sci* **2019**, *20*, doi:10.3390/IJMS20061274.
17. Ray Chaudhuri, A.; Nussenzweig, A. The Multifaceted Roles of PARP1 in DNA Repair and Chromatin Remodelling. *Nat Rev Mol Cell Biol* **2017**, *18*, 610, doi:10.1038/NRM.2017.53.
18. Spiegel, J.O.; Van Houten, B.; Durrant, J.D. PARP1: Structural Insights and Pharmacological Targets for Inhibition. *DNA Repair (Amst)* **2021**, *103*, doi:10.1016/J.DNAREP.2021.103125.
19. Cohen-Armon, M. A Long-Lasting PARP1-Activation Mediates Signal-Induced Gene Expression. *Cells* **2022**, *11*, doi:10.3390/cells11091576.
20. Kuzuhara, T.; Sei, Y.; Yamaguchi, K.; Suganuma, M.; Fujiki, H. DNA and RNA as New Binding Targets of Green Tea Catechins. *J Biol Chem* **2006**, *281*, 17446–17456, doi:10.1074/JBC.M601196200.
21. Chanphai, P.; Tajmir-Riahi, H.A. Structural Dynamics of DNA Binding to Tea Catechins. *Int J Biol Macromol* **2019**, *125*, 238–243, doi:10.1016/j.ijbiomac.2018.12.054.
22. Galindo-Murillo, R.; Cheatham, T.E. Computational DNA Binding Studies of (–)-Epigallocatechin-3-Gallate. *J Biomol Struct Dyn* **2018**, *36*, 3311–3323, doi:10.1080/07391102.2017.1389306.
23. Zheng, X.; Chen, A.; Hoshi, T.; Anzai, J.I.; Li, G. Electrochemical Studies of (-)-Epigallocatechin Gallate and Its Interaction with DNA. *Anal Bioanal Chem* **2006**, *386*, 1913–1919, doi:10.1007/S00216-006-0752-3.
24. Ghosh, K.S.; Sahoo, B.K.; Jana, D.; Dasgupta, S. Studies on the Interaction of Copper Complexes of (-)-Epicatechin Gallate and (-)-Epigallocatechin Gallate with Calf Thymus DNA. *J Inorg Biochem* **2008**, *102*, 1711–1718, doi:10.1016/j.jinorgbio.2008.04.008.
25. Ji, C.; Yin, X.; Duan, H.; Liang, L. Molecular Complexes of Calf Thymus DNA with Various Bioactive Compounds: Formation and Characterization. *Int J Biol Macromol* **2021**, *168*, 775–783, doi:10.1016/J.IJBIOMAC.2020.11.135.
26. Sriram, M.; Van der Marel, G.A.; Roelen, H.L.P.F.; Van Boom, J.H.; Wang, A.H.J. Conformation of B-DNA Containing O6-Ethyl-G-C Base Pairs Stabilized by Minor Groove Binding Drugs: Molecular Structure of d(CGC[E6G]AATTCGCG Complexed with Hoechst 33258 or Hoechst 33342. *EMBO J* **1992**, *11*, 225–232, doi:10.1002/J.1460-2075.1992.TB05045.X.
27. Arndt Jovin, D.J.; Jovin, T.M. Analysis and Sorting of Living Cells According to Deoxyribonucleic Acid Content. *J Histochem Cytochem* **1977**, *25*, 585–589, doi:10.1177/25.7.70450.
28. Okabe, S.; Suganuma, M.; Hayashi, M.; Sueoka, E.; Komori, A.; Fujiki, H. Mechanisms of Growth Inhibition of Human Lung Cancer Cell Line, PC-9, by Tea Polyphenols. *Jpn J Cancer Res* **1997**, *88*, 639–643, doi:10.1111/J.1349-7006.1997.TB00431.X.
29. Kudryashova, K.S.; Chertkov, O.V.; Nikitin, D.V.; Pestov, N.A.; Kulaeva, O.I.; Efremenko, A.V.; Solonin, A.S.; Kirpichnikov, M.P.; Studitsky, V.M.; Feofanov, A.V. Preparation of Mononucleosomal Templates for Analysis of Transcription with RNA Polymerase Using SpFRET. *Methods in Molecular Biology* **2015**, *1288*, 395–412, doi:10.1007/978-1-4939-2474-5_23.
30. Lyubitelev, A.V.; Kudryashova, K.S.; Mikhaylova, M.S.; Malyuchenko, N.V.; Chertkov, O.V.; Studitsky, V.M.; Feofanov, A.V.; Kirpichnikov, M.P. Change in Linker DNA Conformation upon Histone H1.5 Binding to Nucleosome: Fluorescent Microscopy of Single Complexes. *Moscow Univ Biol Sci Bull* **2016**, *71*, doi:10.3103/S0096392516020061.
31. Buning, R.; Van Noort, J. Single-Pair FRET Experiments on Nucleosome Conformational Dynamics. *Biochimie* **2010**, *92*, 1729–1740, doi:10.1016/j.biochi.2010.08.010.
32. Valieva, M.E.; Armeev, G.A.; Kudryashova, K.S.; Gerasimova, N.S.; Shaytan, A.K.; Kulaeva, O.I.; McCullough, L.L.; Formosa, T.; Georgiev, P.G.; Kirpichnikov, M.P.; et al. Large-Scale ATP-Independent Nucleosome Unfolding by a Histone Chaperone. *Nat Struct Mol Biol* **2016**, *23*, 1111–1116, doi:10.1038/nsmb.3321.
33. Almajano, M.P.; Delgado, M.E.; Gordon, M.H. Changes in the Antioxidant Properties of Protein Solutions in the Presence of Epigallocatechin Gallate. *Food Chem* **2007**, *101*, 126–130, doi:10.1016/J.FOODCHEM.2006.01.009.
34. Zhou, B.R.; Feng, H.; Kale, S.; Fox, T.; Khant, H.; de Val, N.; Ghirlando, R.; Panchenko, A.R.; Bai, Y. Distinct Structures and Dynamics of Chromatosomes with Different Human Linker Histone Isoforms. *Mol Cell* **2021**, *81*, 166-182.e6, doi:10.1016/J.MOLCEL.2020.10.038.
35. Maluchenko, N. V; Nilov, D.K.; Pushkarev, S. V; Kotova, E.Y.; Gerasimova, N.S.; Kirpichnikov, M.P.; Langelier, M.-F.; Pascal, J.M.; Akhtar, M.S.; Feofanov, A. V; et al. Mechanisms of Nucleosome Reorganization by PARP1. *Int J Mol Sci* **2021**, *22*, doi:10.3390/ijms222212127.
36. Lambert, J.D.; Lee, M.J.; Diamond, L.; Ju, J.; Hong, J.; Bose, M.; Newmark, H.L.; Yang, C.S. Dose-Dependent Levels of Epigallocatechin-3-Gallate in Human Colon Cancer Cells and Mouse Plasma and Tissues. *Drug Metab Dispos* **2006**, *34*, 8–11, doi:10.1124/DMD.104.003434.
37. Kiser, J.R.; Monk, R.W.; Smalls, R.L.; Petty, J.T. Hydration Changes in the Association of Hoechst 33258 with DNA. *Biochemistry* **2005**, *44*, 16988–16997, doi:10.1021/BI051769X.

38. Hayat, K.; Iqbal, H.; Malik, U.; Bilal, U.; Mushtaq, S. Tea and Its Consumption: Benefits and Risks. *http://dx.doi.org/10.1080/10408398.2012.678949* **2015**, *55*, 939–954, doi:10.1080/10408398.2012.678949.
39. Guo, Y.; Zhi, F.; Chen, P.; Zhao, K.; Xiang, H.; Mao, Q.; Wang, X.; Zhang, X. Green Tea and the Risk of Prostate Cancer: A Systematic Review and Meta-Analysis. *Medicine* **2017**, *96*, doi:10.1097/MD.0000000000006426.
40. Reygaert, W.C. Green Tea Catechins: Their Use in Treating and Preventing Infectious Diseases. *Biomed Res Int* **2018**, *2018*, doi:10.1155/2018/9105261.
41. Kun, E.; Kirsten, E.; Mendeleyev, J.; Ordahl, C.P. Regulation of the Enzymatic Catalysis of Poly(ADP-Ribose) Polymerase by DsDNA, Polyamines, Mg2+, Ca2+, Histones H1 and H3, and ATP†. *Biochemistry* **2003**, *43*, 210–216, doi:10.1021/BI0301791.
42. Gillooly, J.F.; Hein, A.; Damiani, R. Nuclear DNA Content Varies with Cell Size across Human Cell Types. *Cold Spring Harb Perspect Biol* **2015**, *7*, 1–27, doi:10.1101/CSHPERSPECT.A019091.
43. Malinina, D.K.; Sivkina, A.L.; Korovina, A.N.; McCullough, L.L.; Formosa, T.; Kirpichnikov, M.P.; Studitsky, V.M.; Feofanov, A. V. Hmo1 Protein Affects the Nucleosome Structure and Supports the Nucleosome Reorganization Activity of Yeast FACT. *Cells* **2022**, *11*, doi:10.3390/CELLS11192931.
44. Malyuchenko, N. V.; Koshkina, D.O.; Korovina, A.N.; Gerasimova, N.S.; Kirpichnikov, M.P.; Studitsky, V.M.; Feofanov, A. V. The Effect of Gossypol on the Structure of Nucleosomes. *Moscow Univ Biol Sci Bull* **2020**, *75*, 142–146, doi:10.3103/S0096392520030050.
45. Klinker, H.; Haas, C.; Harrer, N.; Becker, P.B.; Mueller-Planitz, F. Rapid Purification of Recombinant Histones. *PLoS One* **2014**, *9*, doi:10.1371/JOURNAL.PONE.0104029.
46. Zhou, B.R.; Feng, H.; Ghirlando, R.; Li, S.; Schwieters, C.D.; Bai, Y. A Small Number of Residues Can Determine If Linker Histones Are Bound On or Off Dyad in the Chromatosome. *J Mol Biol* **2016**, *428*, 3948–3959, doi:10.1016/J.JMB.2016.08.016.
47. Luger, K.; Rechsteiner, T.J.; Richmond, T.J. Expression and Purification of Recombinant Histones and Nucleosome Reconstitution. *Methods Mol Biol* **1999**, *119*, 1–16, doi:10.1385/1-59259-681-9:1.
48. Gaykalova, D.A.; Kulaeva, O.I.; Bondarenko, V.A.; Studitsky, V.M. Preparation and Analysis of Uniquely Positioned Mononucleosomes. *Methods Mol. Biol.* **2009**, *523*, 109–123.